THE JOURNAL OF PHYSICAL CHEMISTRY B

Article

Ultrafast Dynamics of Polarons in Conductive Polyaniline: Comparison of Primary and Secondary Doped Forms

Jeongho Kim, Sungnam Park, and Norbert F. Scherer

J. Phys. Chem. B, **2008**, 112 (49), 15576-15587 • Publication Date (Web): 12 November 2008

Ultrafast Dynamics of Polarons in Conductive Polyaniline: Comparison of Primary and Secondary Doped Forms

Jeongho Kim,[†] Sungnam Park,[‡] and Norbert F. Scherer*

Department of Chemistry and The James Franck Institute, University of Chicago, 929 E. 57th St., Chicago, Illinois 60637

Received: May 6, 2008; Revised Manuscript Received: September 12, 2008

Time- and wavelength-resolved pump−probe measurements are performed on the conductive, primary and secondary doped, forms of polyaniline in solution to investigate the relaxation dynamics of photoexcited polarons. Contrasting dynamics observed in the two forms allow investigation of electronic (and structural) relaxation of this material. Pump pulse at 800 nm photoexcites an electron from the valence to polaron band, and subsequent relaxation dynamics are probed by a white light continuum pulse. Three distinct features are observed in the primary doped sample: (1) absorption near time zero in the 900−1025 nm probe wavelength region; (2) delayed absorption from 850 to 1025 nm; (3) pronounced oscillations with frequencies of 165 and 210 cm^{-1}. The first two features are associated with intraband absorptions to higher-lying states in the polaron band from the initial excited and conformationally changed intermediate states. The oscillations reflect torsional motions associated with photoexcitation and relaxation. In the secondary doped material, only bleaching and stimulated emission are observed throughout the whole spectral region; neither transient absorption signals nor oscillatory dynamics are observed. Kinetic modeling is performed to establish the mechanism of relaxation. We propose that the excited polaron relaxes nonradiatively to the ground state through an intermediate state(s) with a twisted geometry. Our measurements and analysis allow us to describe the structure of the polaron bands for primary and secondary doped polyaniline; they are in the small and large polaron limits, respectively, and are consistent with a bandgap for the primary doped form and without a bandgap (i.e., metallic) for the secondary doped material.

I. Introduction

Over the past 30 years, conducting (conjugated) polymers have attracted considerable attention both of fundamental interest and for technological applications.[1−3] Both experiments and simulations have shown that reducing conformational disorder of the subunits enhances conjugation and energy transport.[4,5] Furthermore, defect states formed in the $\pi-\pi^*$ bandgap by p- or n-type doping facilitate conductivity through the π-conjugated backbone.[6,7] Defect states can also play a major role in creating an insulator-to-metal transition.[1,7,8] Therefore, the nature of the electronic excitation in conjugated polymers with nondegenerate ground states is a controversial and unresolved topic. When neutral conjugated polymers are photoexcited (photodoping), the central issue is whether the primary excitation is a mobile charged polaron (pair) or a bound neutral exciton, i.e., a semiconductor band vs molecular exciton model.[9] Much effort has been devoted to determining which excitation is created first and the process for generating mobile charge carriers.[10−21] For example, in polydiacetylene, the primary excitation is a neutral exciton with strong exciton binding energy.[10,11] In contrast, the primary excitation in poly(*p*-phenylenevinylene) (PPV) and its derivatives is debated to be a neutral exciton[12−17] or a charged polaron.[18−21]

By contrast, chemically doped conjugated polymers, which show high electrical conductivity at room temperature, have clearly charged defect (polaron) states that are extrinsically introduced in the bandgap by chemical treatment.[22] In that sense, chemically doped polymers should be contrasted from photodoped polymers, where charge carriers are transiently photogenerated either directly[20] or via a secondary process such as exciton dissociation.[23,24] Thus, in chemically doped polyaniline (PANI), as studied in this work, a polaron is the primary electronic excitation as well as charge carrier. Compared to the extensive research on photodoped semiconducting polymers, there has been a relative lack of studies on photoexcited charge carrier dynamics in chemically doped metallic polymers. The present paper is intended to clearly articulate the changes in relaxation dynamics and electronic structure of polaron states in conductive PANI associated with doping type.

Polarons (or bipolarons) are (a type of) charge carrier defect states that are important in conducting polymers such as polyaniline.[7,25−27] A polaron is an electronic carrier self-trapped in a potential well produced by the deformation of the molecule it occupies.[28] Its energy is determined by electron−phonon coupling through Coulomb interactions.[29,30] Depending on whether long-range or short-range electron−lattice interactions dominate, qualitatively different types of self-trapping occur. A carrier with a long-range interaction self-traps to form a "large" polaron wherein the charge carriers are delocalized over more than a single site.[29,31] This self-trapped state shrinks (localizes) as the strength of the electron−lattice interaction increases. A self-trapped state localized to a single site, termed a "small" polaron, is formed when the electron−lattice interac-

* To whom correspondence should be addressed. E-mail: nfschere@uchicago.edu.

[†] Present address: Department of Chemistry, University of Toronto, Toronto, Ontario M5S 3H6, Canada.

[‡] Present address: Department of Chemistry, Stanford University, Stanford, CA 94305.

10.1021/jp803984f CCC: $40.75
Published on Web 11/12/2008

tion is short-ranged and particularly when the interaction is strong (i.e., strong electron−phonon coupling).[32,33] These two limits have qualitatively different electronic transport properties;[28] the large polaron has significantly higher mobility that decreases with increasing temperature (i.e., metallic behavior) while the small polaron has (very) low mobility that increases with increasing temperature (i.e., semiconducting behavior). The electron−lattice interactions depend to a significant extent on the spatial conformation of the polymer chain and charge distribution therein. The role of the morphology leading to increased conductivity can be investigated through spectroscopic measurements of conducting polymers with varying amounts of order.

This paper, an extension of our earlier publication,[34] is an ultrafast optical investigation of the carrier (i.e., polaron) dynamics of conformationally relaxed polyaniline. Polyaniline (PANI) achieves high conductivity with both chemical doping (i.e., changing its oxidation state by protonation with acids) and chemical modification of its conformational structure. The former, termed primary doping (PD), is a process of adding charges (protons) into the polymer backbone with no change in the number of electrons, leading to the formation of a polaron.[35−38] Films of primary doped PANI exhibit only modest conductivity, e.g., on the order of 10 S/cm.[35] The chemical modification, termed secondary doping (SD), is perhaps better understood as preferential or effective solvation of the high charge density that allows the polymer (of polar monomers) to sample extended conformations rather than compact (contorted) structures driven by the need to solvate its own charges. Secondary doping, in turn, creates a topologically less distorted structure.[39−41] Recently, it was reported that films of secondary doped PANI prepared by a novel synthetic method exhibit the hallmark of metallic conductivity, i.e., a monotonic increase in conductivity with temperature.[42] The achievement of truly metallic polymer samples by a chemically effected structural transition allows the study of an insulator-to-metal transition of the 1D conductor in the small and large polaron limits. Ultrafast optical studies of polaron excitation and relaxation can give further insight into the increased conductivity of secondary doped PANI.

Theoretical studies of the 50% proton-doped (poly)emeraldine salt by Bredas and co-workers[43−45] showed that the polaron states of PANI have an asymmetric electronic structure, which is in contrast to other conducting polymers with nondegenerate ground states. The asymmetric charge conjugation (i.e., the Fermi level does not occur at the center of the π band) and the A−B character of the polymer[46] cause the upper polaron band to be very flat and nearly degenerate with the conduction band. This leaves only one broad polaron band (i.e., the lower polaron band) in the bandgap with the Fermi level at the middle of this half-filled band. The calculations predict[43−45] two transitions to the polaron band from the valence band, at 1.8 and 2.6 eV, with intraband absorption in the IR region. These findings agree with the experimental linear absorption spectrum of PD-PANI.[40] This calculated electronic band structure provides a picture that is important for understanding the conducting behavior of PANI.

In our ultrafast pump−probe study of primary doped PANI (PD-PANI), referred to as paper I,[34] the photoexcited polaron exhibited multiexponential relaxation dynamics ranging over 4 decades of time up to 100 ps. Extensive vibronic activity was observed in these time-resolved pump−probe experiments. Furthermore, unlike many other electro-optic polymers,[47−49] PANI has a very small fluorescence quantum yield, yet complete ground-state recovery occurs on the 100 ps time scale. Therefore, relaxation must occur via an intermediate state or set of states. Martinez and co-workers reported that the photoexcitation of ethylene evolves to a twisted geometry with charge-separated character and nonradiatively quenches to the ground state through a conical intersection.[50] Following this idea, we proposed that photoexcited PANI will relax to a geometrically distorted intermediate state that involves torsional motions between the adjacent rings.[34] The lack of a significant transition dipole from this state facilitates nonradiative recovery to the ground state whose slow rate may reflect motion through a conical intersection.

Paper I presented ultrafast optical pump−probe transient transmission measurements of PD-PANI at a single wavelength, 800 nm. The present paper extends the spectral range of the probe beam over the entire absorption band of PD-PANI and the higher energy (650−1050 nm) region of the near- to mid-IR absorption of secondary doped PANI (SD-PANI). These comparative measurements and a kinetic model analysis give insight into the relaxation dynamics of photoexcited carriers in PANI and changes in the electronic structure of polaron band associated with the insulator−metal transition.

II. Experimental Section

Gaussian pulses, 18 fs in duration and 20 nJ in energy, were generated at 800 nm from a home-built cavity-dumped Ti:sapphire oscillator.[51] These seed pulses were injected into a home-built high-repetition-rate acousto-optic Ti:sapphire regenerative amplifier. The pulses were amplified to 1.2 μJ at repetition rates up to 250 kHz, compressed to 30 fs duration by a dual-grating compressor and a prism pair. The pulse energy available for experiments was 400 nJ. The amplified beam was split by a partial reflecting (50% R) mirror: one beam was used as a pump after prism compensation for material dispersion, and the other was focused into a sapphire disk to generate a white light continuum. The continuum was retroreflected through a prism pair for dispersion compensation, and a slit was set up between the second prism and the retroreflecting mirror to select spectral components with 20−30 nm fwhm bandwidth. These spectrally selected, temporally compressed pulses serve as the probe. 50 and 25 cm focal length doublet lenses were used to focus the pump and probe beams, respectively, into the sample. The sample was contained in a 1 in. diameter, 0.5 mm path length spinning cell rotating at ~10 Hz. The experimental time resolution of 40−50 fs was determined by measuring the sum frequency cross-correlation of the pump and probe beams at the location of the sample.

Signals were acquired by detecting the probe beam transmission through the sample using a pair of Si photodetectors (New Focus, Nirvana 2007). The probe beam was split before the sample, and this reference beam was directed to an identical detector. The DC amplitudes of the probe and reference beams were adjusted to the same level with neutral density filters. The difference of the probe and reference signals was processed in a lock-in amplifier (Stanford Research, SR-830) referenced to a chopper in the pump beam. The lock-in output was sampled 1000 times at each delay step by a 16-bit ADC (National Instruments), and the whole scan was repeated at least 30 times and averaged. The resultant was divided in a computer by the same reference signal sampled by the ADC (DC component) yielding $\Delta T/T$, the fractional change of the transmitted probe intensity induced by the pump pulse. This signal detection scheme was required to obtain the better than one part in 10^5 sensitivity necessary for analysis. The pump-induced probe transmission waveforms depended on the sample excitation rate

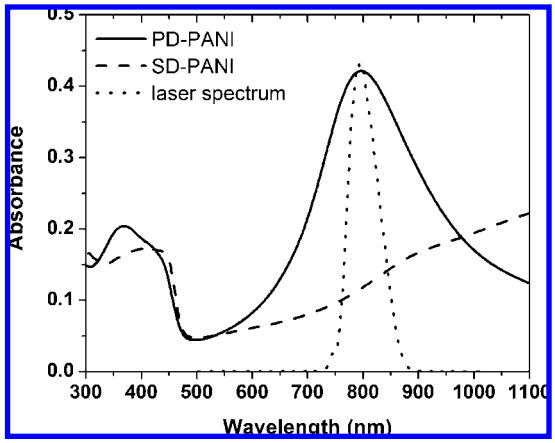

Figure 1. Linear absorption spectra of PD-PANI (solid) and SD-PANI (dashed) and the laser spectrum (dotted) of the pump used in the measurements.

and pulse energy as described in paper I; hence, precautions described therein were applied in the present measurements.[34] For example, the pulse energy and sample excitation rate were attenuated to the level where the measured dynamics no longer depend on excitation power.

Anisotropy data were acquired by orienting a polarizer (Karl Lambrecht, MGTYA-5) in the probe beam at 45° with respect to the pump beam. After the sample, the parallel and perpendicular components of the probe beam were separated by a Rochon polarizer (Karl Lambrecht, MRA-10). Each component was simultaneously detected with two identical Si photodetectors. The signals were then processed with two lock-in amplifiers, numerically averaged as described above and stored in the computer. It was verified that the (initial) anisotropy of the dye molecule IR-140 matched the expected value of 0.4 before and after the anisotropy measurement of PANI.

Primary and secondary doped PANI solutions were prepared by dissolving 4 mg of emeraldine base powder (Polysciences, undoped form) with 5 mg of DL-camphorsulfonic acid in 10 mL of chloroform for PD-PANI and *m*-cresol for SD-PANI. The linear spectra of PANI solutions are unchanged with additional acid, verifying that PANI is fully (i.e., 50%) doped. All the experiments presented here were performed on freshly prepared samples (to avoid formation of aggregated particles) yet after sufficient aging time (overnight) such that the polaron band was fully developed. Further details are given in paper I.[34]

III. Results

Primary Doped PANI. The linear absorption spectra of primary and secondary doped PANI solutions are shown in Figure 1, together with the laser spectrum of the pump beam. The pump−probe transient transmission spectra of PD-PANI at different pump−probe delay times are shown in Figure 2. The pump-induced fractional transmission change ($\Delta T/T$) of the probe beam is measured from −0.5 to 150 ps probe delay in 25 nm intervals from 650 to 1025 nm. The individual transients are shown in Figure 3 in 50 nm wavelength increments to allow more careful inspection. Each of them is fit with third- to fifth-order multiexponentials with a variety of time constants spanning 4 decades from tens of femtoseconds to tens of picoseconds. A stretched exponential is not a good fit to most of the transients other than the 800 nm/800 nm degenerate wavelength case studied in paper I. Instead of applying phenomenological multiexponential fitting, fitted curves obtained

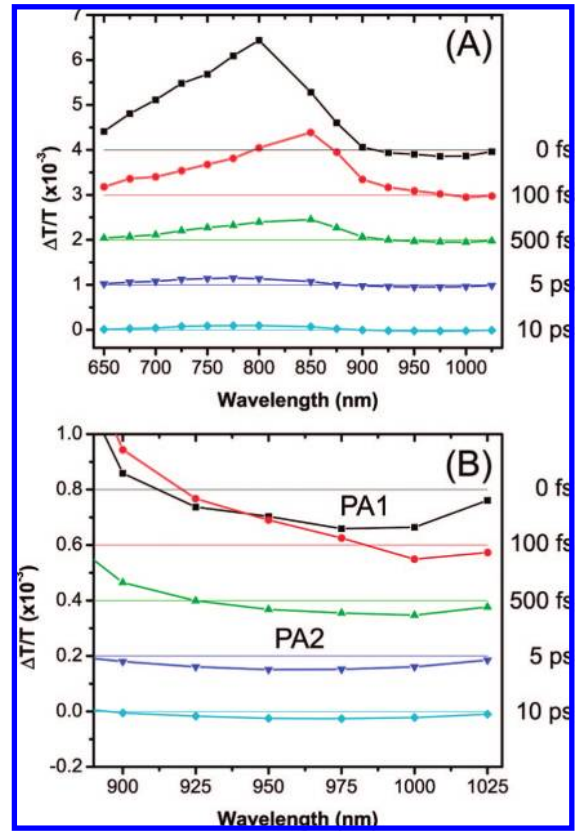

Figure 2. (A) Pump-induced transient transmission spectra of PD-PANI at various pump−probe delay times are shown. The spectra at different delay times are vertically shifted for clarity. The baseline (zero) for each spectrum is shown together. (B) The plot in (A) is magnified in the red side of the absorption peak to emphasize the transient absorption features, **PA1** and **PA2**.

from a kinetic model analysis, which will be described in the next section, are shown together with the pump−probe data.

Two distinctive features can be seen on the red side of the absorption peak (850−1025 nm): first, an early time (i.e., near time zero) negative signal (i.e., absorption) from 900 to 1025 nm, which is labeled as **PA1**; second, a transient absorption on the several to tens of picoseconds time scale, which is labeled as **PA2**. The major transient absorption features observed in the pump−probe data are summarized in Table 1. The pump−probe signal of neat chloroform is measured and subtracted from the PANI solution signal to eliminate the contribution from the pure solvent dispersive response to the near $t = 0$ feature. As a result, Figure 4 shows that the negative (absorptive) signal is enhanced, and small positive peaks at 0.5 ps in the 1000 and 1025 nm signals are eliminated. The second feature is fit by an exponential of negative amplitude with a time constant of ∼10 ps.

The blue side (650−800 nm) exhibits a very fast, sub-picosecond time scale, initial decay followed by a slow decay over 3 decades of time; sub-picoseconds to tens of picoseconds. One notable feature is a "dip" at ∼500 fs to 1 ps observed in the 650−700 nm data shown in Figure 5. This absorptive feature can be fit by a negative-amplitude exponential component, whose time constant gradually increases from 0.6 ps at 700 nm to 2.2 ps at 650 nm. We label this absorption feature as **PA3**.

Oscillations are superimposed on the exponential decay dynamics; these damp out in 2 ps. The oscillations are analyzed by linear prediction singular value decomposition (LPSVD).[52]

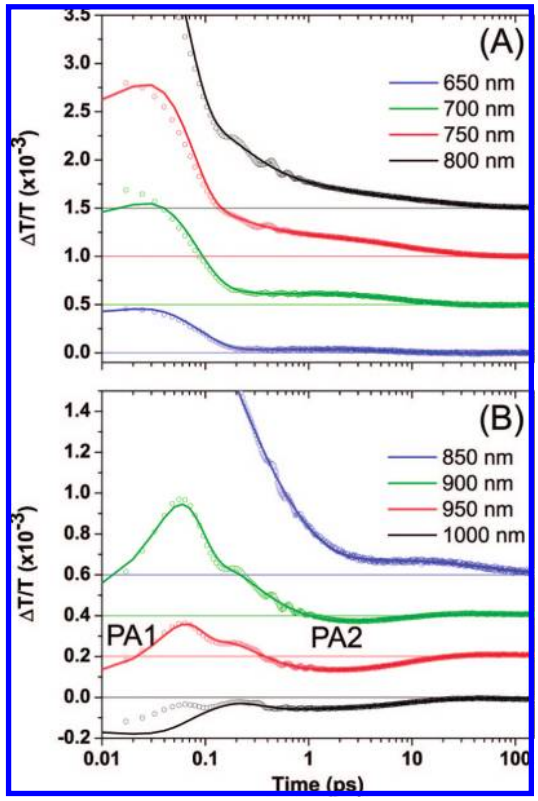

Figure 3. Pump−probe signals (empty dots) of PD-PANI for probe wavelengths of (A) 650−800 nm and (B) 850−1025 nm. Data were recorded every 25 nm but are shown in 50 nm intervals for clarity. The best-fit curves (solid line) obtained from the kinetic analysis are shown together.

TABLE 1: Major Transient Absorption Features in the Pump−Probe Data of PD- and SD-PANI

label	description of transient absorption feature
PA1	transient absorption near time zero in PD-PANI data
PA2	transient absorption at 1−10 ps in PD-PANI data
PA3	transient absorption at ∼0.5 ps in PD-PANI data (absorptive "dip")
SA1	transient absorption near time zero in SD-PANI data

The results are summarized in Table 2. The analysis resolves two dominant frequencies of 165 and 210 cm^{-1} at most wavelengths, especially near the resonance. As shown in Table 2, the phase of the oscillation also shifts by π from below to above the resonance.

Secondary Doped PANI. The pump−probe transient spectra and time-domain pump−probe data of SD-PANI are shown in Figures 6 and 7, respectively. They differ from the pump−probe signals for PD-PANI in several significant ways. (1) Only positive signals (i.e., stimulated emission/ground-state bleaching) are observed on the red side of the absorption peak; neither a distinct negative signal (to be discussed later) nor oscillations are observed. (2) In contrast, on the blue side of the absorption peak, an early time absorption near time zero is observed from 650 to 750 nm, analogous to the **PA1** absorption of PD-PANI. The negative signal increases in magnitude from 750 nm to the blue. We label this absorption feature **SA1**. The pure solvent response of *m*-cresol (not shown), which is only a minor contribution, is also removed from the SD-PANI signal prior to analysis.

Transient Anisotropy. The transient anisotropy is measured for both PD- and SD-PANI to help elucidate the origin of the

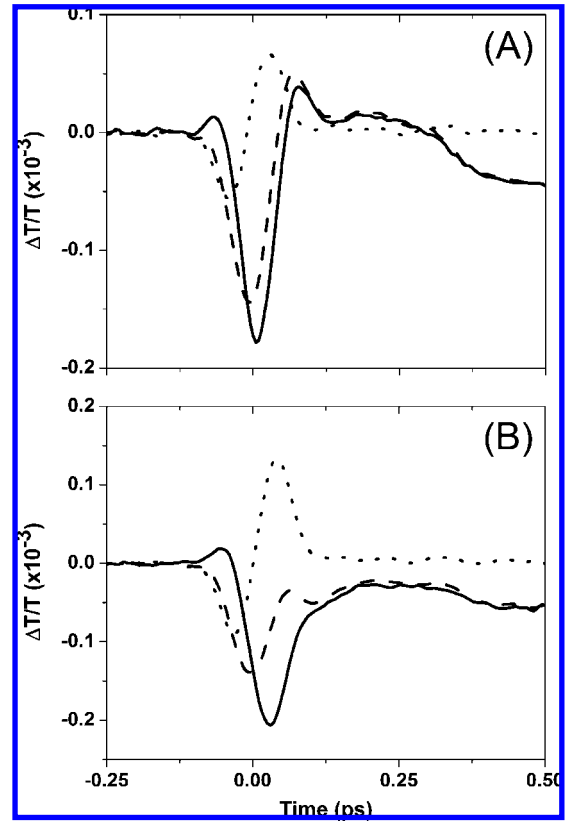

Figure 4. Pure solvent signal (short-dashed) subtracted from the measured PD-PANI solution signal (long-dashed) to give the resultant solution-only signal (solid) at the wavelengths of (A) 975 nm and (B) 1000 nm.

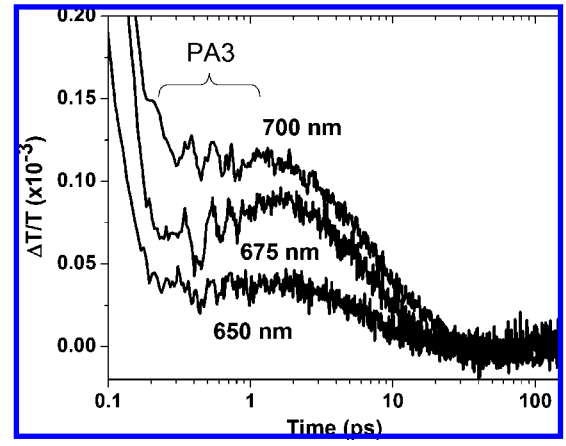

Figure 5. Pump−probe signals of PD-PANI at probe wavelengths of 650−700 nm. Note that there is a "dip" at ∼0.5 ps. This absorptive feature is labeled as **PA3**. This feature should be contrasted from the oscillations arising from vibrational coherence observed in the same time range of 0.3−0.7 ps.

initial fast decay that is especially significant at the resonant wavelength. Figure 8 shows the transient anisotropy

$$r(t) = \frac{S_{\parallel} - S_{\perp}}{S_{\parallel} + 2S_{\perp}} \quad (1)$$

at 800 nm probe wavelength calculated from the pump−probe transient responses, $S(t)$, obtained with parallel and perpendicular polarizations that are shown in the inset. The anisotropy of PD-PANI decays very rapidly from an initial value of 0.33 to 0.14

TABLE 2: LPSVD Analysis Results of Oscillations Observed in the PD-PANI Pump−Probe Signal

probe λ (nm)	freq (cm^{-1})	damping time (ps)	phase (deg)
650	145	0.36	−145
675	161	0.34	171
	211	0.44	−154
700	152	0.17	−171
	200	0.42	−117
725	191	0.30	−81
750	159	0.20	−0.7
775	162	0.20	−28
	213	0.48	15
800	160	0.29	−30
	212	0.49	−2.9
850	166	0.44	−88
	235	0.32	−124
875	168	0.29	−78
	214	0.24	−44
900	168	0.39	−88
	219	0.27	−77
925	167	0.34	−84
	214	0.24	−53
950	161	0.45	−30
	203	0.36	12
975	155	0.83	17
	203	0.43	−347

and remains at that value for at least 3 ps. We fit the fast initial decay by either a 40 fs half-width at half maximum (hwhm) Gaussian or a 30 fs exponential, with the Gaussian giving a better fit. An oscillatory component of 120 cm^{-1} frequency is superimposed on the anisotropy decay as can be seen in the residual obtained by subtracting the Gaussian fit from the data (Figure 8A). In contrast, the anisotropy of SD-PANI increases from an initial value of 0.2 to 0.4 in 250 fs and decays slowly until it reaches a value of 0.28, remaining constant to beyond 3 ps delay. The anisotropy is fit by a rising exponential with a 120 fs time constant, a decaying exponential with a 1.1 ps time constant, and a constant offset of 0.26. No oscillations are evident.

IV. Kinetic Modeling of Relaxation

A kinetic model was developed to establish a quantitative relaxation mechanism. As shown in Figure 9, the three-level scheme involving the ground (G), excited (E), and intermediate (I) states, which was used to fit the 800 nm pump−probe signal in paper I,[34] was modified to address the greater range of behaviors observed in the present wavelength-resolved

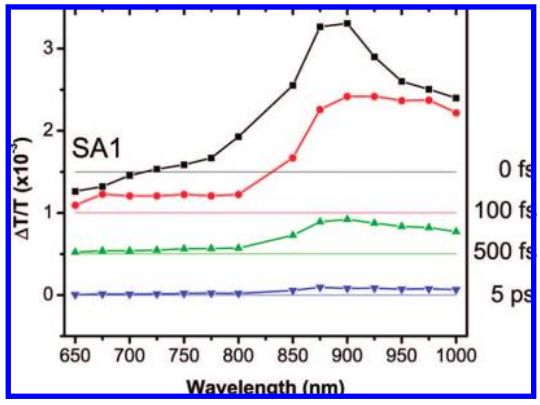

Figure 6. Pump-induced transient transmission spectra of SD-PANI at various pump−probe delay times are shown. The spectra at different delay times are vertically shifted for clarity.

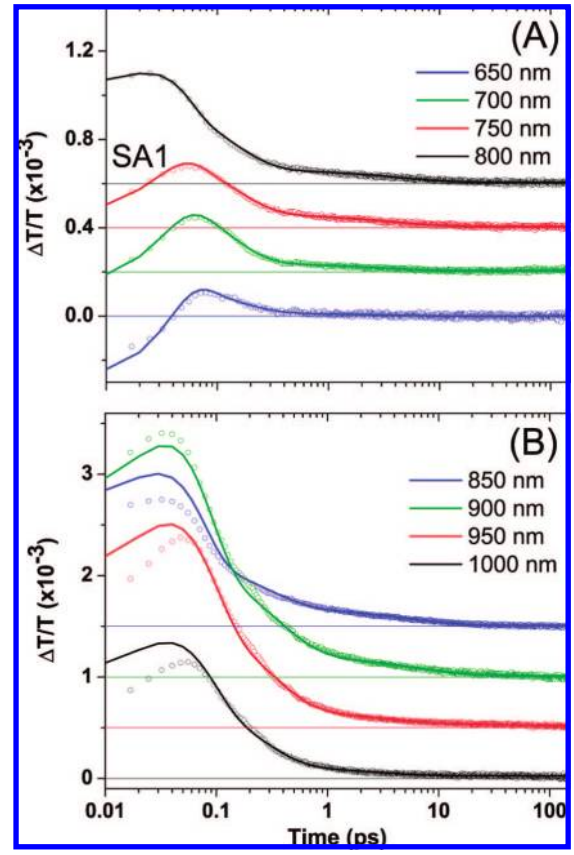

Figure 7. Pump−probe transients of SD-PANI for probe wavelengths of (A) 650−800 nm and (B) 850−1025 nm in 50 nm increments. Each data was fit using the kinetic analysis described in the text.

signals. To account for excited-state absorption features (**PA1**, **PA2**, **PA3**, and **SA1**) observed in the experimental data, higher-lying excited states were added to the scheme: E_2 and E_u for the absorption from E and I_2 for absorption from I. In this modified model, each additional fitting parameter was added until the data over the entire spectral range were adequately fit so that the number of fitting parameters is kept to a minimum.

The kinetic differential equations based on the scheme described in Figure 9 are given in the Appendix. They were solved to give the populations of each state, and the model signal was constructed from 40 fs to 150 ps at each wavelength. The instrument response function (IRF) was deconvoluted from the measured pump−probe signal, and the model signal was fit to the IRF-deconvoluted signal using the Levenberg−Marquardt nonlinear least-squares fitting algorithm[53] (Mathcad, Mathsoft) by minimizing the sum of the squared deviations. Then, using the parameters obtained, the model signal (i.e., a combination of exponentials) was convoluted with the IRF and refit to the measured signal. In this manner, we were able to more effectively fit the ultrafast initial pump−probe response that was complicated by a negative component attributed to excited-state absorption. Most of experimental data were well fit by the simulated signals, even to the tens of femtoseconds time scale.

Three relaxation processes were taken into account to adequately fit the experimental data with this model: (1) inhomogeneity of the excited-state energy, (2) electronic and/or vibrational cooling in the E state, and (3) population relaxation to an intermediate. First, the inhomogeneity of the excited-state energy, which was already addressed in paper I, arises from the structural variations and conformational disorder

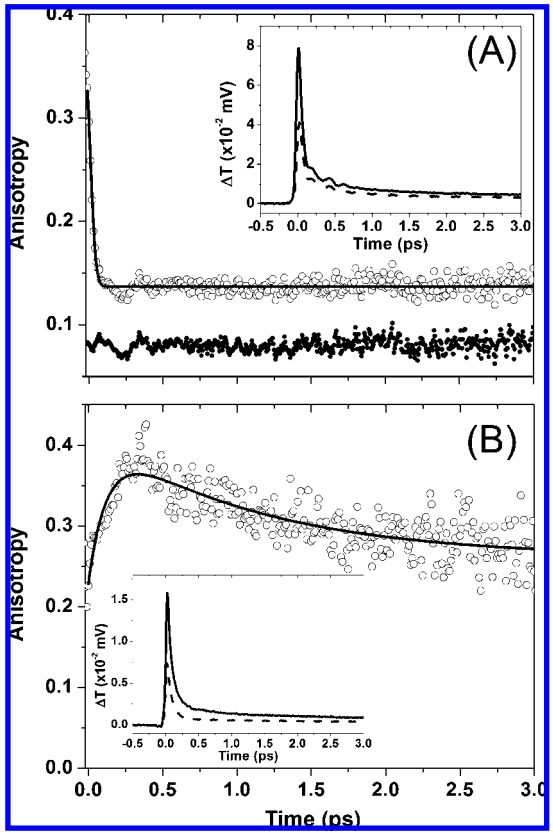

Figure 8. Transient anisotropy (empty points) and its fit (solid line) for (A) PD-PANI and (B) SD-PANI at 800 nm probe wavelength. PD-PANI anisotropy was fit by a Gaussian of 80 fs fwhm with a constant offset (0.14). The residual obtained by subtracting the Gaussian fit from the data is also plotted with an offset (filled points). SD-PANI anisotropy was fit by an asymptotically increasing exponential (τ = 190 fs) and a decaying exponential (τ = 580 fs) with a constant offset (0.28). Insets are the transient pump−probe transient transmission data measured with the polarization of the probe beam parallel (solid) and perpendicular (dashed) to the pump beam. The data are shown only up to 3 ps to emphasize the early time dynamics. The anisotropy decay continues in a simple monotonic fashion thereafter.

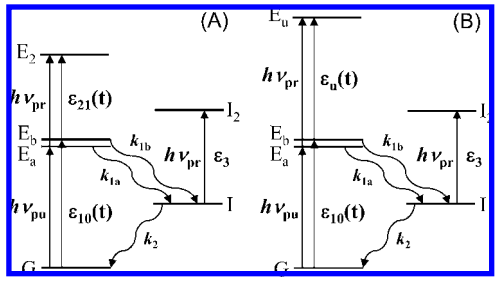

Figure 9. Kinetic models used to simulate the relaxation dynamics of (A) PD-PANI and (B) SD-PANI.

of conjugated segments and chemical defects inherently present in the polymer chains. Many possible cases were considered in the analysis. We found that it was sufficient to consider the inhomogeneity of energy in the first excited state (E) to adequately fit the data over the entire spectral range. Since the first excited state in our model corresponds to the polaron band, inhomogeneity in the first excited-state energy should fit within the width of polaron band. For example, the bandwidth of the polaron band in PD-PANI was theoretically predicted to be ~1.1 eV.[43]

Second, the rapid changes in the extinctions of the transitions associated with cooling in the first excited state were considered.

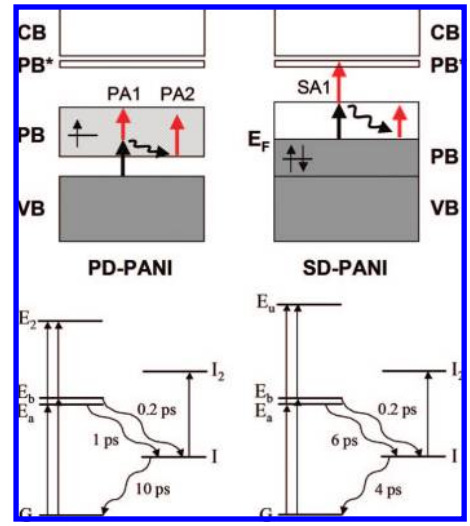

Figure 10. Proposed band structures of PD- and SD-PANI in the small and large polaron limits, respectively, depending on the interaction between polaron units. VB: valence band; PB: lower polaron band; PB*: upper polaron band; CB: conduction band. The light- and dark-shaded regions refer to the energy states of unpaired and paired spins, respectively. Black and red arrows represent the interactions with pump and probe, respectively. Major transient absorption features (**PA1**, **PA2**, and **SA1**) are shown. For both PD- and SD-PANI, the energy gap between valence and upper polaron/conduction band is predicted to be 3.4 eV (360 nm) or larger from the linear absorption spectrum. The width of the lower polaron band in PD-PANI is ~1.8 eV (650 nm), and the half-width of the lower polaron band in SD-PANI is ~1.5 eV (800 nm).

Including time-dependent stimulated emission/ground-state bleaching allowed fitting the sub-100 fs fast decay in the pump−probe data. To do so, we defined a time-dependent extinction of the ground state to first excited state transition (ε_{10}) in the form of eq A.5 in the Appendix. This component is associated with rapid spectral shift of the stimulated emission due to electronic/vibrational cooling of the excited population. By employing the time-dependent extinction, population relaxation through a manifold of excited states is modeled in a simple way without introducing many states.

Also, a term to account for time-dependent excited-state absorption was required, especially to fit the ultrafast decaying early time transient absorption, **PA1**, on the red side (900−1050 nm) of the absorption peak in the PD-PANI signal. It is described by defining the time- and wavelength-dependent extinction for the excited-state absorption (ε_{21}) in the form of eq A.6 to account for both decaying and accumulating populations due to cooling. This term was only considered for PD-PANI since the transient absorption near time zero was only observed in the PD-PANI signals.

Finally, population decay was described by first-order kinetics. It should be noted that the absorption from I to I_2 was needed to adequately fit the SD-PANI data even though transient absorption (i.e., negative signal) on long time scales, analogous to the **PA2** absorption of the PD-PANI signal, is not observed in the pump−probe signal of SD-PANI.

The proposed band structure of conductive PANI, based on the band structure calculations for the polaron lattice of PANI,[43,45] is schematically illustrated in Figure 10 together with the results of kinetic modeling. The upper and lower polaron bands exist as defect states in the bandgap between the valence and conduction bands. Because of the asymmetric chemical composition of PANI backbone, the upper polaron band is narrow and nearly degenerate with the conduction band. The

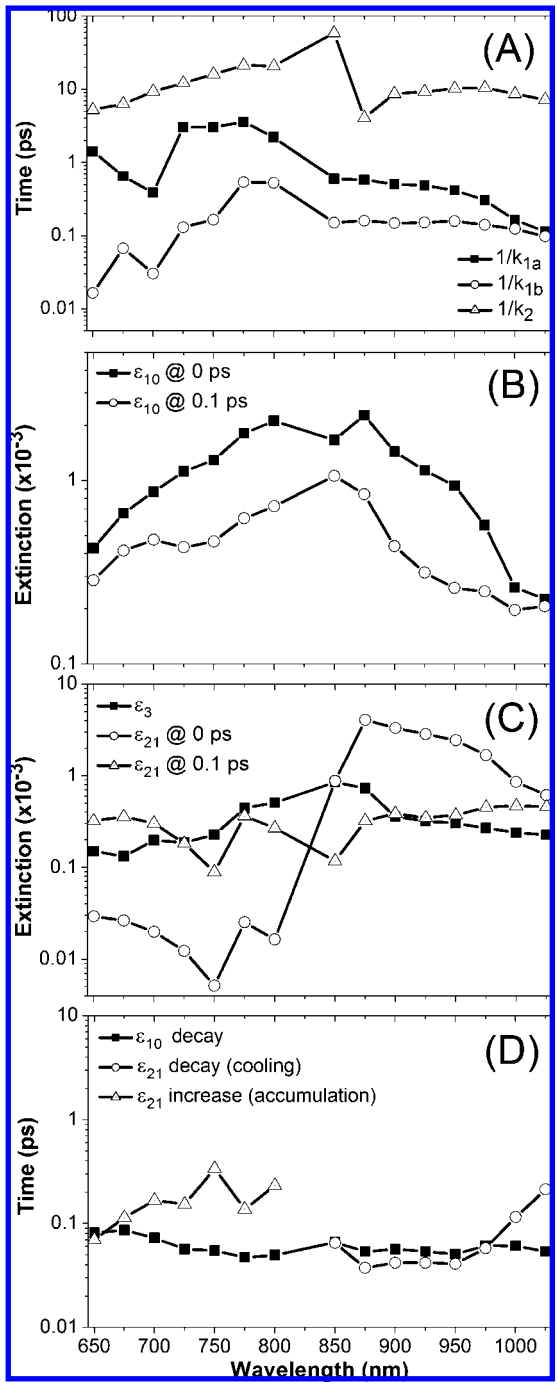

Figure 11. Best-fit parameters of the kinetic model for PD-PANI. (A) Relaxation time constants, k_{1a}^{-1} (square, solid), k_{1b}^{-1} (circle, dashed), and k_2^{-1} (triangle, dotted) of E_a, E_b, and I states, respectively. (B) Spectral profile of the extinction, $\varepsilon_{10}(t)$, at 0 ps (square, solid) and 0.1 ps (circle, dashed). (C) The extinction (ε_3) for the transition from I to I_2 (square, solid) and spectral profile of the extinction, $\varepsilon_{21}(t)$, at 0 ps (circle, dashed) and 0.1 ps (triangle, dotted). (D) Time constants for decay of $\varepsilon_{10}(t)$ (square, solid) (hwhm of a Gaussian describing the ε_{10} decay), decay of $\varepsilon_{21}(t)$ (circle, dashed), and increase of $\varepsilon_{21}(t)$ (triangle, dotted) in the first excited state (E_a and E_b).

lower polaron band is half-filled and has a significant bandwidth. The details of the band structure, for example, comparison of electronic structures of PD- and SD-PANI, will be further discussed in the next section. From now on, the results of the spectroscopic measurements and kinetic modeling will be discussed based on the band structures just described.

A. PD-PANI. The best-fit kinetic model parameters for PD-PANI are presented in Figure 11. The decay times of each state are shown in Figure 11A. The analysis introduces inhomogeneity by considering two relaxation paths on different time scales: a slow path, from E_a to I, on the time scale of several picoseconds, and a fast path, from E_b to I, on a sub-picoseconds time scale. The intermediate state (I) is found to have a lifetime of about 10 ps, consistent with the presence of a long-lived intermediate state. However, some inconsistencies (i.e., nonmonotonic trends) were observed in the rate constant values at different probe wavelengths. This might indicate a limitation of our model, which was sufficient to capture the dynamics observed in all of our data, but may be an oversimplified representation of the complicated electronic structure of this conjugated polymer. As shown in Figure 11B, the extinction, ε_{10}, for the transition from G to E_a and E_b, decreases very rapidly. Figure 11D summarizes these Gaussian decays with their half-widths at half-maximum (hwhm) ranging from 60 to 90 fs. The decay is clearly slower than the instrument response function (~45 fs fwhm Gaussian). This rapid initial decay, which is especially prominent on the blue side of the absorption peak, is attributed to rapid cooling of the initially excited population in the first excited state, i.e., polaron band in Figure 10. Figure 11C shows the rapid decay and blue shift of the extinction, ε_{21}, for the transition from E (E_a and E_b) to E_2. It suggests that fast electronic/vibrational cooling occurs in the first excited state (polaron band) on the 50−500 fs time scale; the decay constants are shown in Figure 11D. This is the origin of both the **PA1** and **PA3** absorption features. The early time absorption, **PA1**, is observed at red wavelengths, while the delayed absorption, **PA3**, appears at blue wavelengths as the population cools to lower states. Figure 11C also shows that the extinction, ε_3, for the I to I_2 transition has significant amplitude from 800 nm to the near-IR region. This extinction is responsible for **PA2** absorption and is attributed to an intraband absorption within the polaron band, as shown in Figure 10.

B. SD-PANI. An analogous model was applied to SD-PANI except that, instead of E_2 in PD-PANI, another excited state (E_u) is considered to explain the **SA1** absorption observed from 750 nm to beyond 650 nm. This absorption is considered a transition of different character from the **PA1** absorption of PD-PANI. In Figure 10, **SA1** is attributed to absorption to the upper polaron band and/or conduction band (i.e., an interband transition). The best-fit parameters are shown in Figure 12. The rate constants shown in Figure 12A exhibit similar trends as in PD-PANI, i.e., kinetic inhomogeneity that is modeled with two relaxation paths from the first excited state on very different time scales. The extinction, ε_{10}, is clearly red-shifted from that of PD-PANI as can be seen in Figure 12B, suggesting that the energy of the polaron band is lowered upon secondary doping, as depicted in Figure 10. As in PD-PANI, the initial rapid decay is described by 60−90 fs hwhm Gaussians (Figure 12D). This is attributed to rapid cooling of the initially excited population in the first excited state (polaron band) as in PD-PANI. The profile of the intermediate state absorption, ε_3, shown in Figure 12C, is red-shifted compared with that of PD-PANI and looks very similar to the profile of ε_{10}. This suggests that transient absorption from the intermediate, similar to **PA2** absorption of PD-PANI, can be hidden under the more prominent red-shifted bleaching/stimulated emission. The transition from the first excited-state to the higher-lying state, E_u, also shown in Figure 12C, exhibits an absorption profile that increases from 800 nm to the blue. This absorption decays very rapidly and vanishes on a 100 fs time scale. This rapid decay, with time constants shown in Figure 12D, is also due to electronic/vibrational

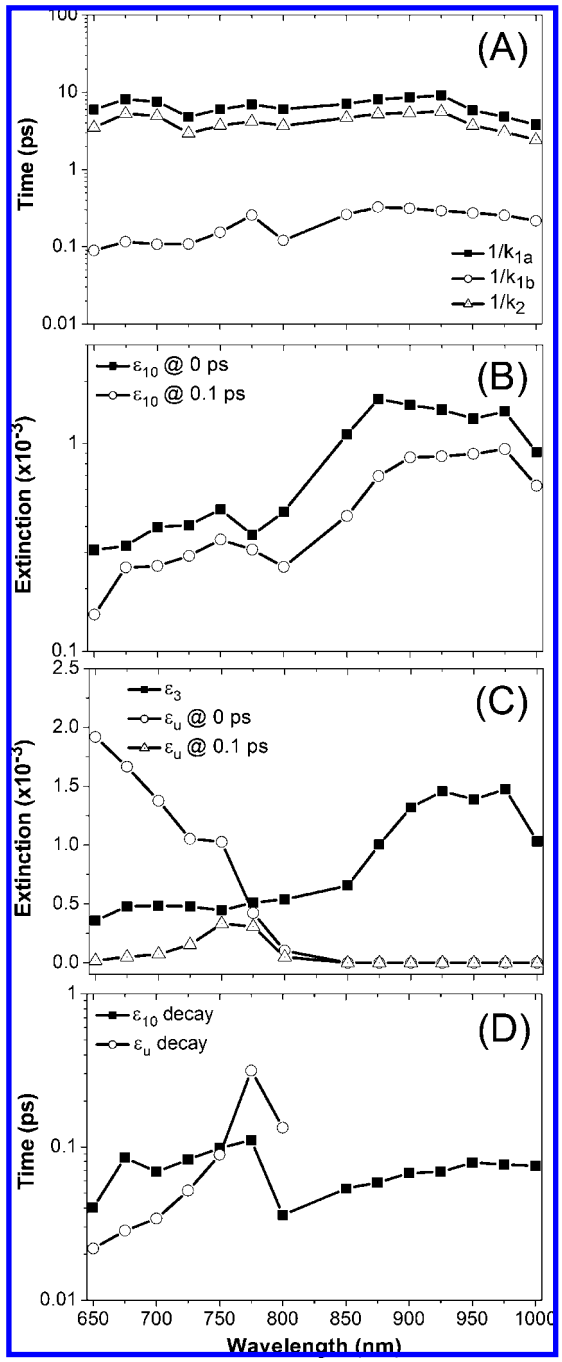

Figure 12. Best-fit parameters of the kinetic model for SD-PANI. (A) Relaxation time constants, k_{1a}^{-1} (square, solid), k_{1b}^{-1} (circle, dashed), and k_2^{-1} (triangle, dotted) of E_a, E_b, and I states, respectively. (B) Time evolution of the extinction, $\varepsilon_{10}(t)$, at 0 ps (square, solid) and 0.1 ps (circle, dashed). (C) The extinction (ε_3) for the transition from I to I_2 (square, solid) and spectral profile of the extinction, $\varepsilon_u(t)$, at 0 ps (circle, dashed) and 0.1 ps (triangle, dotted). (D) Time constants for decay of $\varepsilon_{10}(t)$ (square, solid) (hwhm of a Gaussian describing the ε_{10} decay) and decay of $\varepsilon_u(t)$.

cooling in the first excited state such that the transition shifts out of the probe spectral range.

V. Discussion

Structural Changes Associated with an Insulator−Metal Transition. The insulator-to-metal transition of PANI induced by chemical doping involves strong electron−phonon coupling, i.e., correlation between the geometric and electronic structure of the polymer.[37,54−56] The electron−phonon coupling will reflect changes in the ring torsion angles[57−59] as well as bond lengths. The ring torsions play an important role in determining the energy and geometry of PANI.[59] Since the formation of the doping-induced defects (polaron and bipolaron) involves substantial ring torsional motion, recovery of the ground-state geometry may be slowed. Considering the fact that the bleach signal persists over 150 ps and the quantum yield for radiative emission in PANI is immeasurably small, the decay of the excitation in PANI must occur nonradiatively through an intermediate state. Indeed, photoinduced absorption experiments have shown a very long lifetime of the defect states generated upon photoexcitation.[60−63] The intermediate state(s) can be probed by transient absorption to a higher-lying state; the absorption observed in the pump−probe data gives direct evidence of the presence of intermediate states. Therefore, the transient absorption on sub-picoseconds to tens of picoseconds time scales observed from 850 to 1025 nm, as shown in Figures 2 and 3, is associated with a long-lived photoexcited polaron state. Furthermore, judging from the width of the polaron band that was estimated to be ~1.1 eV,[43] this transient absorption is an intraband absorption in the polaron band (see Figure 10).

Two dominant oscillatory contributions of 165 and 210 cm^{-1} are observed in the PD-PANI pump−probe signals. These frequencies agree with the N−ring−N deformation modes reported in Raman and IR studies of the emeraldine base form of PANI.[64] The presence of these oscillations implies two things: (1) strong electron−phonon coupling is associated with photoexcitation of the polaron, and (2) torsional motions are coupled to the relaxation process of the photoexcited polaron. The former is characteristic of the "small polaron" case.[65] The oscillatory component of 120 cm^{-1} frequency observed in the anisotropy decay of PD-PANI further supports strong electron−phonon coupling in PD-PANI.

In contrast, no oscillation is observed in the pump−probe signals of SD-PANI. Thus, the coupling of torsional motions to the excitation (and perhaps relaxation) is diminished. Secondary doping gives rise to extended (i.e., less defective) molecular conformations resulting from better charge solvation in the polymer chain by a more (di)polar solvent.[40] This elongates the π conjugation length and improves excitation and charge delocalization over the polymer chain. We presume that this give rise to the greater mobility of charge carriers in SD-PANI. These characteristics correspond to the "large polaron" case with weak electron−phonon coupling.[65]

Origin of Initial Fast Dynamics. The transient anisotropies of PD- and SD-PANI exhibited very different decay behaviors. The fast Gaussian decay of PD-PANI anisotropy was already addressed in paper I.[34] The structural disorder and chemical defects inherent in the polymer mean that the polymer consists of conjugated segments of different effective chain lengths, thereby introducing a distribution of energies. The fast initial decay is attributed to rapid localization of the excitation into low-energy segments, a process that is enhanced by strong electron−phonon coupling. Thus, there is a rapid randomization of the associated transition dipole orientations to an anisotropy value of 0.14. This is the same conclusion reported for the time-resolved fluorescence of polysilane.[66,67]

In contrast, the transient anisotropy of SD-PANI shows an initial increase, which is not possible for a nondegenerate two-level transition.[68,69] If there is a negative contribution to the pump−probe signal from excited-state absorption, the anisotropy can have any value and becomes complicated.[70] We believe the transient absorption from the lower polaron band to the upper

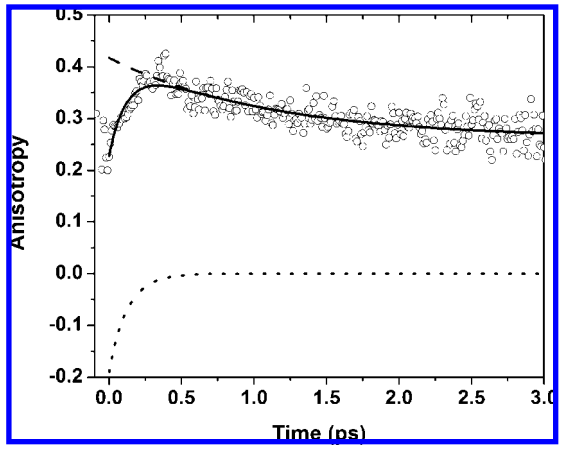

Figure 13. Two components contributing to the transient anisotropy (empty circles) of SD-PANI. A biexponential fit (solid) can be decomposed into a decaying exponential with a constant offset (dashed) and a rising exponential (dotted) as described in the text.

polaron band (Figure 10) could give a negative contribution to the initial anisotropy. In the kinetic modeling, the excited-state transient absorption to a higher-lying state (E_u) is found to decay with a 100 fs exponential time constant (Figure 12D). The contribution of this component to the initial anisotropy of SD-PANI becomes evident in Figure 13, where the SD-PANI anisotropy is fit by two exponentials (with a constant offset). One is a 120 fs exponential rise from an initial value of −0.2 to 0 that is attributed to the excited-state absorption from the first to the second excited state. If the orientation of the transition dipole for the first to second excited state transition is orthogonal to the transition dipole for the ground to first excited state transition, the initial anisotropy value for the transition between the two states is −0.2. As the transient absorption shifts out of the probe spectral window due to cooling on the 100 fs time scale, the anisotropy approaches a value close to 0.4, as in a nondegenerate two-level system with parallel transition dipoles.

The other component is an exponential decay from the initial value of 0.4 to an asymptotic value of 0.26 with a time constant of 1.1 ps. This slow decay relative to that observed for the PD-PANI anisotropy could arise from incoherent hopping of the excitation between conjugated segments along the chain. Compared to PD-PANI, SD-PANI has a longer average conjugation length resulting from spatially expanded coil conformations, which allows migration of the excitation along the less distorted chain. When the initial excitation that is delocalized over a relatively small portion of a chain (i.e., excitation at blue edge of the absorption band) migrates along the chain, the anisotropy decreases since a new distribution of chain orientations are populated. This slow decay of the anisotropy suggests that the excitation in SD-PANI diffuses over a significant distance before being localized in low-energy segments and thus explains the enhanced conductivity of SD-PANI over PD-PANI. In contrast, the more randomly coiled chains and shorter conjugation lengths of PD-PANI restrict the initial excitation to diffuse only small distances and to cause randomization of the transition dipole orientations of those conjugated segments. Therefore, the anisotropy would decay rapidly.

Band Structure Perspective. To understand the conduction mechanism, it is important to determine the electronic structure of conductive PANI, especially of the polaron states. Electron spin resonance (ESR) measurements of conductive PANI[55,56,71−73] established that two kinds of spin states, i.e., Curie and Pauli spins, are involved in the doping process. The ESR intensity increases together with conductivity at the early stages of doping because the polarons created are considered to be isolated such that every polaron contributes to the ESR signal. This type of local spin state is termed a (paramagnetic) Curie spin. At increasing doping levels, the ESR intensity decreases (from the maximum) while conductivity continues to increase. In this case, the high concentration of polarons form a polaron lattice and the originally isolated spin states merge together to form an energy band whose lower half is filled. These spin states are termed Pauli spins, which have a *g*-value close to free electrons and are a signature of metallic behavior. Since only spins around the Fermi level of a metal contribute to the ESR signal, the intensity is expected to decrease with the conversion of Curie spins to Pauli spins with increased doping. Also, it was reported that the Pauli spin contribution to the magnetic susceptibility increases with increased doping level.[55,56]

Considering variation in lengths of conjugated segments and interactions between them, polaron states in a single polymer chain can be described in terms of a band picture (see Figure 10). Here, the band refers to an inhomogeneously broadened density of states distribution. Although a molecular exciton description for the electronic structure of neutral conjugated polymers has gained more credibility recently, a semiconductor band description is still valid for chemically doped (charged) conjugated polymers, where charge carrier states are permanently present in the bandgap.[22] On the basis of the band structure calculations for the polaron lattice of emeraldine salt PANI,[43,45] the ESR measurements summarized above, and our measurements, we propose a model for the energy structure of doped PANI in terms of a semiconductor band model. This is illustrated in Figure 10. The half-filled lower polaron band, which directly takes part in conduction, can have two limits depending on the strength of the interaction between polaron units: (1) when the polaron−polaron interaction is weak, polaron states are isolated and localized such that a group of half-filled localized polaron states with (paramagnetic) Curie spins become the highest-occupied band—this is associated with the small polaron limit; (2) when the polaron−polaron interaction is strong, the polaron states merge to form a polaron lattice with a half-filled band with (paired hence spinless) Pauli spins. In this case, polarons are well delocalized over the conjugation length—the large polaron limit.

A. PD-PANI. The proposed band structure of PD-PANI shown in Figure 10 qualitatively accounts for the results of the ultrafast pump−probe measurements and kinetic modeling. The polaron band structure of PD-PANI resembles the small polaron limit; despite the high doping level (50%), the polarons are rather isolated from each other due to the structural (twist) defects between the aromatic rings that exist in the compact coil. Upon optical excitation with a short (impulsive) pump pulse, a portion of the valence band population is promoted to half-occupied states in the lower polaron band, leaving holes in the valence band. This gives a bleach contribution to the pump−probe signal. The excited population is then immediately excited by the probe pulse to the higher half-occupied states within the lower polaron band (intraband absorption), giving the early time PA1 absorption between 900 and 1025 nm seen in Figures 2 and 3. Then, the population promoted to the polaron band vibrationally and/or electronically cools to lower unoccupied states in the band, and the probe absorption rapidly blue-shifts as seen in Figure 11C. As the excited population relaxes through the lower energy states, the bleaching/stimulated emission components decay. This population proceeds through intermedi-

ate state(s) that are probed by PA2 absorption to higher unoccupied states (within the polaron band). This "intermediate state" persists in PD-PANI on the tens of picoseconds time scale at 900 nm and redder probe wavelengths.

The PA3 absorption observed at ~500 fs in the 650−700 nm pump−probe data of Figure 5 can arise from (1) intraband absorption subsequent to cooling or (2) absorption to a higher-lying state, that is, the upper polaron band/conduction band. Case 1 is reasonable in that the delayed absorption is observed on the blue side (650−700 nm), but it requires that the polaron band have a large bandwidth of at least 1.8 eV (650 nm), which is more than 50% larger than the predicted value of 1.1 eV from the calculation by Bredas.[43,45] Case 2 is possible in terms of the energy difference between the lower polaron band and upper polaron/conduction band. From the absorption spectrum of PD-PANI,[74] the gap between the valence and conduction band is predicted to be ~3.4 eV (360 nm). Therefore, after excitation by the 800 nm pump (1.5 eV), an excited-state absorption is expected at 1.9 eV (630 nm) probe energy. This approximately matches the wavelengths where the PA3 absorption was observed. However, the transition to the upper polaron band should not occur at a delayed time of ~500 fs, but near time zero. Thus, we attribute the PA3 absorption in PD-PANI to intraband absorption subsequent to cooling. In other words, the E_2 state corresponds to a state within the polaron band. The discrepancy in the width of the lower polaron band from the calculation by Bredas[43] can be attributed to the absence of structural disorder, intrachain interaction (in a coiled chain), and Coulomb interactions with counterions in the calculation. These factors can make significant contributions to the electronic structure and energies.

B. SD-PANI. In contrast to PD-PANI, SD-PANI should have a polaron band in the large polaron limit due to the strong interaction between polarons that can occur in expanded coil conformations (Figure 10). This picture is consistent with linear visible/infrared spectra, conductivity, and solution ESR measurements.[40,74,75] Chemically transforming PD-PANI to SD-PANI improves the interaction between polaron units as a result of π-delocalization. Consequently, the number of long-chain segments in a distribution of conjugated chain lengths (i.e., distribution of energy levels) increases, giving rise to energy lowering (and possibly broadening) of the polaron band.[45] It even leads to closing of the energy gap between the valence and lower polaron band, as suggested by MacDiarmid.[74] This change can be seen in the absorption spectra in Figure 1: Upon secondary doping, the polaron absorption at 800 nm decreases, while the free carrier tail in the near- and mid-IR range increases. Also, the 3.4 eV (360 nm) absorption of PD-PANI disappears in SD-PANI. Transitions from the top of the valence band cannot occur due to closing of the gap between the valence and polaron bands. Only transitions from the Fermi level of the polaron band within the band (free carrier tail) and to the upper polaron/conduction band occur. The identical profiles of stimulated emission/bleaching (ε_{10}) and intermediate state absorption (ε_3) in the kinetic modeling (Figure 12B) support this idea. For the same reason, the absence of intraband absorption near time zero at red wavelengths (analogous to **PA1** of PD-PANI) suggests that the absorption is red-shifted out of the probe spectral detection window because the pump pulse excites the population to nearly the upper edge of the polaron band.

The lack of transient absorption on long time scales (cf. **PA2** feature of PD-PANI), which is the explicit evidence of the intermediate state, can be interpreted in two ways: (1) it is red-shifted out of the probe spectral window since the polaron band of SD-PANI has a smaller bandwidth for intraband relaxation than that of PD-PANI due to formation of the half-filled band with Pauli spins; (2) it still exists but is hidden under the red-shifted bleaching/stimulated emission. The kinetic modeling supports the latter case since the pump−probe signals were adequately fit only with the contribution of the intermediate state absorption. However, considering the limitations of our kinetic model, this point still needs further investigation to confirm the presence of the intermediate state in the SD-PANI photophysics.

In contrast to PD-PANI, transient absorption, **SA1**, was observed near time zero at 750 nm and bluer. This observation means that we are probing the red edge of the transition. Intraband absorption cannot have a red edge so this transient absorption in SD-PANI is to a higher-lying state. Considering the electronic structure of PANI,[43] the transition is to the upper polaron/conduction band as depicted in Figure 10. The kinetic modeling shows that the absorption decays out of the probed spectral window within 500 fs due to cooling (Figure 12D).

VI. Conclusion

Ultrafast pump−probe experiments performed on two conductive forms of PANI enabled a better understanding of the fast relaxation dynamics of photoexcited polarons and changes in polaron band structure accompanying secondary doping. The ultrafast relaxation dynamics measured for chemically doped PANI are attributed to charged polarons. This is in contrast to the dynamics measured for photodoped neutral conjugated polymers, which contain contributions from other excitation species, for example, excitons. Pump−probe signals of both forms of PANI showed multiexponential decay dynamics, ranging to hundreds of picoseconds, which are typical of disordered organic solids and are in agreement with the polaron recombination dynamics of other nondegenerate ground-state conjugated polymers, e.g., polythiophene[76,77] and PPV.[21,78] To account for the multiexponential polaron relaxation dynamics, in our earlier paper, we proposed that an intermediate associated with a structural distortion of the polymer backbone to form a polaron is involved in the relaxation of the photoexcited polaron.[34] The present work clearly reveals the presence of an intermediate state in the transient absorption signals of PD-PANI. Also, the involvement of significant ring-torsional motion in the relaxation process is supported by oscillations observed in the pump-induced probe transmission signals. This is a hallmark of strong electron−phonon coupling in the small polaron case. On the other hand, the presence of an intermediate state was not explicitly evident in the pump−probe signal of SD-PANI, although the kinetic model analysis required one. The transient absorption from the intermediate state might be "hidden" under the red-shifted bleaching/stimulated emission contribution (Figure 11B,C). The lack of any oscillatory component in the pump−probe data of SD-PANI implies that weak torsional motions are involved, which is consistent with weak electron−phonon coupling as expected in the large polaron case.

From the pump−probe measurements and their kinetic modeling, we propose a model for the band structures of PD- and SD-PANI that is consistent with their structural and electrical properties.[40] In PD-PANI, a distribution of half-filled polaron states in the $\pi-\pi^*$ bandgap have more isolated polaron character due to weak polaron−polaron interactions. In contrast, secondary doping gives rise to reduced disorder and enhanced π delocalization through the polymer chain. The stronger interactions between adjacent polarons cause the (polaron) states to merge to form a polaron band with the Fermi level in the

middle of the band and the lower half of the band having merged with the valence band (Figure 10). Since the HOMO and the LUMO are then in contact with each other as in metals, free carriers can transport along the chain by thermal activation, thus rendering significantly enhanced conductivity than in PD-PANI.

Acknowledgment. This research was supported by the University of Chicago MRSEC, the NSF-NIRT program (NSF-ERC-0303389), and NSF grant (CHE 0616663). We thank Dr. Andrew Moran for helpful discussions. N.F.S. thanks the John S. Guggenheim Memorial Foundation for a fellowship.

Appendix

Since the kinetic scheme is not typically found in the literature, it is useful to summarize the pertinent kinetic equations. As shown in Figure 9, there are four states to consider with associated first-order differential rate equations:

$$\frac{d[G]}{dt} = k_2[I] \tag{A.1a}$$

$$\frac{d[E_a]}{dt} = -k_{1a}[E_a] \tag{A.1b}$$

$$\frac{d[E_b]}{dt} = -k_{1b}[E_b] \tag{A.1c}$$

$$\frac{d[I]}{dt} = -k_{1a}[E_a] + k_{1b}[E_b] - k_2[I] \tag{A.1d}$$

These equations are solved with the boundary conditions at $t = 0$:

$$[G]_0 = 0; \quad [E_a]_0 + [E_b]_0 = 1; \quad [I]_0 = 0 \tag{A.2}$$

The resulting time-dependent populations for each state are

$$[E_a] = [E_a]_0 e^{-k_{1a}t} \tag{A.3a}$$

$$[E_b] = [E_b]_0 e^{-k_{1b}t} \tag{A.3b}$$

$$[I] = \frac{k_{1a}}{k_2 - k_{1a}}[E_a]_0(e^{-k_{1a}t} - e^{-k_2t}) + \frac{k_{1b}}{k_2 - k_{1b}}[E_b]_0(e^{-k_{1b}t} - e^{-k_2t}) \tag{A.3c}$$

$$[G] = \frac{k_2}{k_2 - k_{1a}}[E_a]_0(1 - e^{-k_{1a}t}) + \frac{k_2}{k_2 - k_{1b}}[E_a]_0(1 - e^{-k_{1b}t}) + \left(\frac{k_{1a}}{k_2 - k_{1a}}[E_a]_0 + \frac{k_{1b}}{k_2 - k_{1b}}[E_b]_0\right)(e^{-k_2t} - 1) \tag{A.3d}$$

Considering ground state (G) bleaching, stimulated emission from the excited state (E), excited state (E) absorption, and intermediate state (I) absorption as possible contributions, the optical response, $S(t)$, can be constructed from eqs A.3a−A.3d:

$$S(t) = \varepsilon_{10}(t)(1 - [G] + \varepsilon_{10}(t))([E_a] + [E_b]) - \varepsilon_{21}(t)([E_a] + [E_b]) - \varepsilon_3[I]$$

$$= \varepsilon_{10}(t)\Bigg[1 + [E_a]_0 e^{-k_{1a}t} + [E_b]_0 e^{-k_{1b}t} + \frac{k_2}{k_2 - k_{1a}}[E_a]_0(e^{-k_{1a}t} - 1) + \frac{k_2}{k_2 - k_{1b}}[E_a]_0(e^{-k_{1b}t} - 1) + \left(\frac{k_{1a}}{k_2 - k_{1a}}[E_a]_0 + \frac{k_{1b}}{k_2 - k_{1b}}[E_b]_0\right)(1 - e^{-k_2t})\Bigg] - \varepsilon_{21}(t)([E_a]_0 e^{-k_{1a}t} + [E_b]_0 e^{-k_{1b}t}) - \varepsilon_3\Bigg[\frac{k_{1a}}{k_2 - k_{1a}}[E_a]_0 \times (e^{-k_{1a}t} - e^{-k_2t}) + \frac{k_{1b}}{k_2 - k_{1b}}[E_b]_0(e^{-k_{1b}t} - e^{-k_2t})\Bigg] \tag{A.4}$$

The extinctions, ε_{10} and ε_{21}, are regarded as time-dependent functions that are defined with a Gaussian and an exponential, respectively.

$$\varepsilon_{10}(t) = (\varepsilon_{10}^0 - \varepsilon_{10}^1)\exp(-k_d{}^2t^2) + \varepsilon_{10}^1 \tag{A.5}$$

$$\varepsilon_{10}(t) = (\varepsilon_{21}^0 - \varepsilon_{21}^1)\exp(-k_v t) + \varepsilon_{21}^1 \tag{A.6}$$

where the superscripts of the extinctions, 0 and 1, represent their initial and final values, respectively.

For SD-PANI, the transition to the upper polaron band, E_u, is considered instead of a transition to E_2. Thus, we replaced ε_{21} by ε_u, giving a contribution to the signal in the form of

$$S_{upper}(t) = -\varepsilon_u(t)([E_a] + [E_b]) \tag{A.7}$$

where $\varepsilon_u(t) = \varepsilon_u^0 \exp(-k_u t)$.

References and Notes

(1) Shirakawa, H.; Louis, E. J.; MacDiarmid, A. G.; Chiang, C. K.; Heeger, A. J. *Chem. Commun.* **1977**, *578*.
(2) Chiang, C. K.; Fincher, C. R., Jr.; Park, Y. W.; Heeger, A. J.; Shirakawa, H.; Louis, E. J. *Phys. Rev. Lett.* **1977**, *39*, 1098.
(3) Heeger, A. J. *Synth. Met.* **2002**, *125*, 23.
(4) Tretiak, S.; Mukamel, S. *Chem. Rev.* **2002**, *102*, 3171.
(5) Schwartz, B. J. *Annu. Rev. Phys. Chem.* **2003**, *54*, 141.
(6) Bredas, J. L.; Street, G. B. *Acc. Chem. Res.* **1985**, *18*, 309.
(7) Heeger, A. J.; Kivelson, S.; Schrieffer, J. R.; Su, W.-P. *Rev. Mod. Phys.* **1988**, *60*, 781.
(8) Su, W.-P.; Schrieffer, J. R.; Heeger, A. J. *Phys. Rev. Lett.* **1979**, *42*, 1698.
(9) *Primary Photoexcitations in Conjugated Polymers: Molecular Exciton versus Semiconductor Band Model*; Sariciftci, N. S., Ed.; World Scientific: Singapore, 1997; p 640.
(10) Kobayashi, T.; Yoshizawa, M.; Stamm, U.; Taiji, M.; Hasegawa, M. *J. Opt. Soc. Am. B* **1990**, *7*, 1558.
(11) Pakbaz, K.; Lee, C. H.; Heeger, A. J.; Hagler, T. W.; McBranch, D. *Synth. Met.* **1994**, *64*, 295.
(12) Kersting, R.; Lemmer, U.; Mahrt, R. F.; Leo, K.; Kurz, H.; Bassler, H.; Gobel, E. O. *Phys. Rev. Lett.* **1993**, *70*, 3820.
(13) Yan, M.; Rothberg, L. J.; Papadimitrakopoulos, F.; Galvin, M. E.; Miller, T. M. *Phys. Rev. Lett.* **1994**, *72*, 1104.
(14) Leng, J. M.; Jeglinski, S.; Wei, X.; Benner, R. E.; Vardeny, Z. V. *Phys. Rev. Lett.* **1994**, *72*, 156.
(15) Graupner, W.; Cerullo, G.; Lanzani, G.; Nisoli, M.; List, E. J. W.; Leising, G.; De Silvestri, S. *Phys. Rev. Lett.* **1998**, *81*, 3259.
(16) Kraabel, B.; Klimov, V. I.; Kohlman, R.; Xu, S.; Wang, H.-L.; McBranch, D. W. *Phys. Rev. B* **2000**, *61*, 8501.
(17) Muller, J. G.; Lemmer, U.; Feldmann, J. *Phys. Rev. Lett.* **2002**, *88*, 147401.
(18) Lee, C. H.; Yu, G.; Moses, D.; Heeger, A. J. *Phys. Rev. B* **1994**, *49*, 2396.

(19) Frolov, S. V.; Gellermann, W.; Vardeny, Z. V.; Ozaki, M.; Yoshino, K. *Synth. Met.* **1997**, *84*, 493.
(20) Moses, D.; Dogariu, A.; Heeger, A. J. *Phys. Rev. B* **2000**, *61*, 9373.
(21) Miranda, P. B.; Moses, D.; Heeger, A. J. *Phys. Rev. B* **2001**, *64*, 081201.
(22) Furukawa, Y. *J. Phys. Chem.* **1996**, *100*, 15644, and references therein.
(23) Arkhipov, V. I.; Emelianova, E. V.; Bassler, H. *Phys. Rev. Lett.* **1999**, *82*, 1321.
(24) Silva, C.; Stevens, M. A.; Russel, D. M.; Setayesh, S.; Mullen, K.; Friend, R. H. *Synth. Met.* **2001**, *116*, 9.
(25) Su, W.-P.; Schrieffer, J. R. *Proc. Natl. Acad. Sci. U.S.A.* **1980**, *77*, 5626.
(26) Campbell, D. K.; Bishop, A. R. *Phys. Rev. B* **1981**, *24*, 4859.
(27) Bredas, J. L.; Themans, B.; Fripiat, J. M.; re, J. M.; Chance, R. R. *Phys. Rev. B* **1984**, *29*, 6761.
(28) Emin, D. *Phys. Rev. B* **1993**, *48*, 13691.
(29) Holstein, T. *Ann. Phys.* **1959**, *8*, 325.
(30) Toyozawa, Y. *Prog. Theor. Phys.* **1961**, *26*, 29.
(31) Frohlich, H. *Adv. Phys.* **1954**, *3*, 325.
(32) Emin, D.; Holstein, T. *Phys. Rev. Lett.* **1976**, *36*, 323.
(33) Emin, D. *Adv. Phys.* **1973**, *22*, 57.
(34) Kim, J.; Unterreiner, A.-N.; Rane, S.; Park, S.; Jureller, J.; Book, L.; Liau, Y.-H.; Scherer, N. F. *J. Phys. Chem. B* **2002**, *106*, 12866.
(35) MacDiarmid, A. G.; Chiang, J. C.; Halpern, M.; Huang, W. S.; Mu, S. L.; Somasiri, N. L. D.; Wu, W.; Yaniger, S. I. *Mol. Cryst. Liq. Cryst.* **1985**, *121*, 173.
(36) Chiang, J. C.; MacDiarmid, A. G. *Synth. Met.* **1986**, *13*, 193.
(37) MacDiarmid, A. G.; Chiang, J. C.; Richter, A. F.; Epstein, A. J. *Synth. Met.* **1987**, *18*, 285.
(38) Ray, A.; Richter, A. F.; MacDiarmid, A. G.; Epstein, A. J. *Synth. Met.* **1989**, *29*, E151.
(39) MacDiarmid, A. G.; Epstein, A. J. *Synth. Met.* **1994**, *65*, 103.
(40) MacDiarmid, A. G.; Epstein, A. J. *Synth. Met.* **1995**, *69*, 85.
(41) Avlyanov, J. K.; Min, Y.; MacDiarmid, A. G.; Epstein, A. J. *Synth. Met.* **1995**, *72*, 65.
(42) Lee, K.; Cho, S.; Park, S. H.; Heeger, A. J.; Lee, C.-W.; Lee, S.-H. *Nature (London)* **2006**, *441*, 65.
(43) Stasfstrom, S.; Bredas, J. L.; Epstein, A. J.; Woo, H. S.; Tanner, D. B.; Huang, W. S.; MacDiarmid, A. G. *Phys. Rev. Lett.* **1987**, *59*, 1464.
(44) Stasfstrom, S.; Bredas, J. L. *J. Mol. Struct.* **1989**, *188*, 393.
(45) Libert, J.; Bredas, J. L.; Epstein, A. J. *Phys. Rev. B* **1995**, *51*, 5711.
(46) Rice, M. J.; Mele, E. J. *Phys. Rev. Lett.* **1982**, *49*, 1455.
(47) Burroughes, J. H.; Bradley, D. D. C.; Brown, A. R.; Marks, R. N.; Mackay, K.; Friend, R. H.; Burns, P. L.; Holmes, A. B. *Nature (London)* **1990**, *347*, 539.
(48) Baigent, D. R.; Greenham, N. C.; Gruner, J.; Marks, R. N.; Friend, R. H.; Moratti, S. C.; Holmes, A. B. *Synth. Met.* **1994**, *67*, 3.
(49) Perepichka, I. F.; Perepichka, D. F.; Meng, H.; Wudl, F. *Adv. Mater.* **2005**, *17*, 2281.
(50) Ben-Nun, M.; Martinez, T. J. *Chem. Phys. Lett.* **1998**, *298*, 57.
(51) Liau, Y.-H.; Unterreiner, A.-N.; Arnett, D. C.; Scherer, N. F. *Appl. Opt.* **1999**, *38*, 7386.
(52) Vohringer, P.; Scherer, N. F. *J. Phys. Chem.* **1995**, *99*, 2684.
(53) More, J. J.; Garbow, B. S.; Hillstrom, K. E. *User's Guide to MINPACK I*; Argonne National Laboratory: Argonne, IL, 1980; Vol. 80−74.
(54) Ginder, J. M.; Epstein, A. J.; MacDiarmid, A. G. *Synth. Met.* **1989**, *29*, E395.
(55) Epstein, A. J.; Ginder, J. M.; Zuo, F.; Bigelow, R. W.; Woo, H. S.; Tanner, D. B.; Richter, A. F.; Huang, W. S.; MacDiarmid, A. G. *Synth. Met.* **1987**, *18*, 303.
(56) Ginder, J. M.; Richter, A. F.; MacDiarmid, A. G.; Epstein, A. J. *Solid State Commun.* **1987**, *63*, 97.
(57) Stasfstrom, S.; Bredas, J. L. *Synth. Met.* **1986**, *14*, 297.
(58) Ginder, J. M.; Epstein, A. J.; MacDiarmid, A. G. *Solid State Commun.* **1989**, *72*, 987.
(59) Ginder, J. M.; Epstein, A. J. *Phys. Rev. B* **1990**, *41*, 10674.
(60) Roe, M. G.; Ginder, J. M.; Wigen, P. E.; Epstein, A. J.; Angelopoulos, M.; MacDiarmid, A. G. *Phys. Rev. Lett.* **1988**, *60*, 2789.
(61) Sariciftci, N. S.; Smilowitz, L.; Cao, Y.; Heeger, A. J. *J. Chem. Phys.* **1993**, *98*, 2664.
(62) Kim, K.; Blatchford, J. W.; Gustafson, T. L.; MacDiarmid, A. G.; Epstein, A. J. *Synth. Met.* **1995**, *69*, 247.
(63) McCall, R. P.; Ginder, J. M.; Leng, J. M.; Ye, H. J.; Manohar, S. K.; Masters, J. G.; Asturias, G. E.; MacDiarmid, A. G.; Epstein, A. J. *Phys. Rev. B* **1990**, *41*, 5202.
(64) Colomban, P.; Folch, S.; Gruger, A. *Macromolecules* **1999**, *32*, 3080.
(65) Alexandrov, A. S.; Mott, N. *Polarons & Bipolarons*; World Scientific: Singapore, 1995.
(66) Thorne, J. R. G.; Ohsako, Y.; Repinec, S. T.; Abrash, S. A.; Zeigler, J. M.; Hochstrasser, R. M. *J. Lumin.* **1990**, *45*, 295.
(67) Hochstrasser, R. M.; Pereira, M. A.; Share, P. E.; Sarisky, M. J.; Kim, Y. R.; Repinec, S. T.; Sension, R. J.; Thorne, J. R. G.; Iannone, M.; Diller, R.; Anfinrud, P. A.; Han, C.; Lian, T.; Locke, B. *Proc. Indian Acad. Sci. (Chem. Sci.)* **1991**, *103*, 351.
(68) Fleming, G. R. *Chemical Applications of Ultrafast Spectroscopy*; Oxford University Press: Oxford, UK, 1985.
(69) Wynne, K.; Hochstrasser, R. M. *Chem. Phys.* **1993**, *171*, 179.
(70) Jonas, D. M.; Lang, M. J.; Nagasawa, Y.; Joo, T.; Fleming, G. R. *J. Phys. Chem.* **1996**, *100*, 12660.
(71) Javadi, H. H. S.; Laversanne, R.; Epstein, A. J.; Kohli, R. K.; Scherr, E. M.; MacDiarmid, A. G. *Synth. Met.* **1989**, *29*, E439.
(72) Lapkowski, M.; Genies, E. M. *J. Electroanal. Chem.* **1990**, *279*, 157.
(73) Zhuang, L.; Zhou, Q.; Lu, J. *J. Electroanal. Chem.* **2000**, *493*, 135.
(74) Xia, Y.; Wiesinger, J. M.; MacDiarmid, A. G. *Chem. Mater.* **1995**, *7*, 443.
(75) Cao, Y.; Heeger, A. J. *Synth. Met.* **1992**, *52*, 193.
(76) McBranch, D.; Hays, A.; Sinclair, M.; Moses, D.; Heeger, A. J. *Phys. Rev. B* **1990**, *42*, 3011.
(77) Vardeny, Z. V. *J. Mol. Struct.* **1993**, *292*, 279.
(78) Sakamoto, A.; Nakamura, O.; Yoshimoto, G.; Tasumi, M. *J. Phys. Chem. A* **2000**, *104*, 4198.

JP803984F